

# Bandwidth-disorder phase diagram of half doped layered manganites

R. Mathieu<sup>[†]</sup>,<sup>1</sup> M. Uchida,<sup>1</sup> Y. Kaneko,<sup>1</sup> J. P. He,<sup>1</sup> X. Z. Yu,<sup>1</sup> R. Kumai,<sup>2</sup>  
T. Arima,<sup>1,3</sup> Y. Tomioka,<sup>2</sup> A. Asamitsu,<sup>1,4</sup> Y. Matsui,<sup>1,5</sup> and Y. Tokura<sup>1,2,6</sup>

<sup>1</sup>*Spin Superstructure Project (ERATO-SSS), JST, AIST Central 4, Tsukuba 305-8562, Japan*

<sup>2</sup>*Correlated Electron Research Center (CERC), AIST Central 4, Tsukuba 305-8562, Japan*

<sup>3</sup>*Institute of Multidisciplinary Research for Advanced Materials, Tohoku University, Sendai 980-8577, Japan*

<sup>4</sup>*Cryogenic Research Center (CRC), University of Tokyo, Bunkyo-ku, Tokyo 113-0032, Japan*

<sup>5</sup>*Advanced Materials Laboratory, National Institute for Materials Science (NIMS), Tsukuba 305-0044, Japan*

<sup>6</sup>*Department of Applied Physics, University of Tokyo, Tokyo 113-8656, Japan*

(Dated: February 6, 2008)

Phase diagrams in the plane of  $r_A$  (the average ionic radius, related to one-electron bandwidth  $W$ ) and  $\sigma^2$  (the ionic radius variance, measuring the quenched disorder), or “bandwidth-disorder phase diagrams”, have been established for perovskite manganites, with three-dimensional (3D) Mn-O network. Here we establish the intrinsic bandwidth-disorder phase diagram of half-doped layered manganites with the two-dimensional (2D) Mn-O network, examining in detail the “mother state” of the colossal magnetoresistance (CMR) phenomenon in crystals without ferromagnetic instability. The consequences of the reduced dimensionality, from 3D to 2D, on the order-disorder phenomena in the charge-orbital sectors are also highlighted.

PACS numbers: 71.27.+a, 75.47.-m

Half-doped perovskite manganites with small bandwidth  $W$  and small amount of disorder like  $\text{Pr}_{0.5}\text{Ca}_{0.5}\text{MnO}_3$  ( $\text{Pr}^{3+}$  and  $\text{Ca}^{2+}$  being small and similar in size) exhibit a long-range charge and orbital order[1, 2] (CO-OO). This CO-OO, which is associated with the spin ordering (so-called CE-type structure[3]), is schematically illustrated in the top-left panel of Fig. 1. As for the spin sector, the structure is essentially composed of ferromagnetic zig-zag chains antiferromagnetically coupled to one-another. A fragment of such a zig-zag chain is highlighted in the figure. If the disorder becomes larger due to the ion size mismatch of  $R^{3+}$  and  $A^{2+}$ , as in  $\text{Gd}_{0.5}\text{Sr}_{0.5}\text{MnO}_3$ , or  $\text{Eu}_{0.5}\text{Ba}_{0.5}\text{MnO}_3$ , only the short-range CO-OO order is observed[2, 4], producing a “CE-glass” state[4, 5, 6]. Interestingly, the colossal magnetoresistance effect was found to arise from within this coarse-grained homogeneous CE-glass state[6, 7]. In the layered systems, the  $\text{MnO}_2$  planes ( $ab$ -planes) are isolated by two blocking ( $R/A$ )O layers, so that the CO-OO correlation is limited by the two-dimensional (2D) character of the Mn network. Yet,  $\text{La}_{0.5}\text{Sr}_{1.5}\text{MnO}_4$  is a well-known half-doped single-layered manganite with concomitant charge and orbital ordering[8] near 220K. The spin sector orders antiferromagnetically (AFM) at  $T_N=110\text{K}$ [8]. Akin to the perovskite case, crystals with smaller bandwidth such as  $\text{Pr}_{0.5}\text{Ca}_{1.5}\text{MnO}_4$  (PCMO) show CO-OO transitions above room temperature[9]. However, no other half-doped RSMO system seems to exhibit a long-range CO-OO. A CE-glass state is observed in crystals with larger quenched disorder, such as  $\text{Eu}_{0.5}\text{Sr}_{1.5}\text{MnO}_4$ [10] ( $\text{Eu}^{3+}$  is smaller than  $\text{La}^{3+}$ , which is already smaller than  $\text{Sr}^{2+}$ ). In the present article, using high-quality single crystals of  $R_{0.5}A_{1.5}\text{MnO}_4$  manganites, we investigate the CE-glass

state and its location in the plane of quenched disorder vs. bandwidth. The quenched disorder associated with the solid solution of the  $A$ -site cations[4] is quantified using the ionic radius variance  $\sigma^2 = \sum_i x_i r_i^2 - r_A^2$ , according to the scheme devised by Attfield[11].  $x_i$  and  $r_i$  are the fractional occupancies ( $\sum_i x_i=1$ ) and electronic radii of the different  $i$  cations on the  $A$ -site, respectively, and  $r_A = \sum_i x_i r_i$  represents the average  $A$ -site ionic radius, related to the bandwidth.

High quality single crystals of the  $A$ -site disordered  $R_{0.5}\text{Ca}_{1.5}\text{MnO}_4$  (RCMO),  $R_{0.5}\text{Sr}_{1.5}\text{MnO}_4$  (RSMO), and  $R_{0.5}(\text{Ca}_{1-y}\text{Sr}_y)_{1.5}\text{MnO}_4$  (RCSMO) manganites were grown by the floating zone method ( $R = \text{La}, \text{La}_{1-y}\text{Pr}_y, \text{Pr}, \text{Nd}, \text{La}_{0.5}\text{Eu}_{0.5} (\sim \text{Nd}), \text{Sm}, \text{or Eu}$ , while  $A=\text{Ca}, \text{Ca}_{1-y}\text{Sr}_y$ ). The phase-purity of the crystals was checked by x-ray diffraction and the cation concentrations of some of the crystals were confirmed by inductively coupled plasma (ICP) spectroscopy. The ac-susceptibility  $\chi(\omega = 2\pi f)$  data was recorded as a function of the temperature  $T$  and frequency  $f$  on a MPMSXL SQUID magnetometer equipped with the ultra low-field option (low frequencies) and a PPMS6000 (higher frequencies) from Quantum Design, after carefully zeroing or compensating the background magnetic fields of the systems. The resistivity  $\rho$  of the crystals was measured using a standard four-probe method on a PPMS6000, feeding the electrical current in the  $ab$ -plane. The single-crystal x-ray data was recorded at 370K on a Rigaku SPD curved imaging plate system at the beam line BL-1A of the Photon Factory, KEK, Japan. Thin specimens were prepared for observation with transmission electron microscopes (TEMs) by  $\text{Ar}^+$  ion milling at low temperatures, to perform the electron diffraction (ED) measurements, and collect the selected-area electron diffraction patterns (EDPs) and

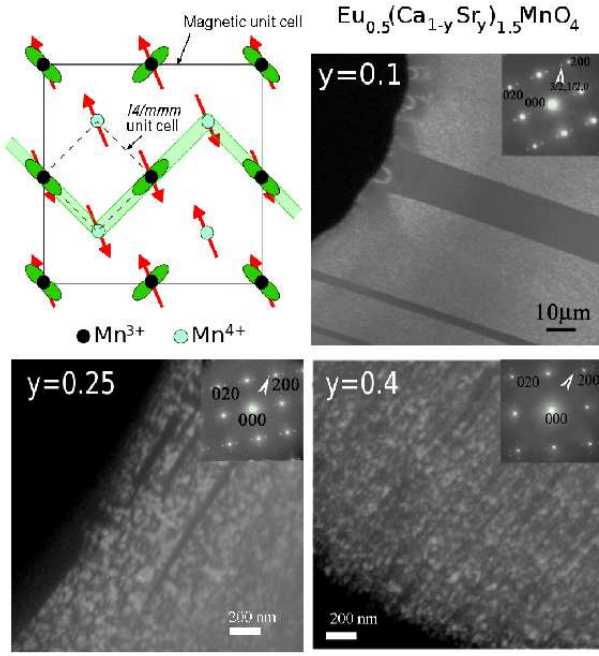


FIG. 1: (color online) Dark field images of  $\text{Eu}_{0.5}(\text{Ca}_{1-y}\text{Sr}_y)_{1.5}\text{MnO}_4$ , illustrating the long-range CO-OO order for  $y=0.1$  and  $y=0.25$  and the short-range CO-OO state for  $y=0.4$ ;  $T = 80\text{K}$ . The corresponding electron diffraction patterns (EDPs, see main text), indexed based on a tetragonal cell with  $a \sim 3.8 \text{ \AA}$  and  $c \sim 12.4 \text{ \AA}$  for simplicity, are shown on the right-top corners of the respective panels. A schematic view of the CE-type structure in the basal plane of the tetragonal structure is also depicted. The orbital order involves staggered  $3x^2 - r^2/3y^2 - r^2$  orbitals of the  $e_g$ -like electrons of  $\text{Mn}^{3+}$ , represented as green (dark gray) lobes in the figure. The spins, represented with red (dark gray) arrows, order ferromagnetically along zig-zag chains, a fragment of which is highlighted in light green (light gray) in the figure.

dark-field (DF) images. The structural modulation wave vector  $q = a^*[\delta \delta 0]$  ( $a$  is the lattice constant,  $aa^*=1$ ) was determined at different temperatures.

$\text{Eu}_{0.5}\text{Ca}_{1.5}\text{MnO}_4$  (ECMO) is very similar to PCMO, albeit a larger variance ( $\sigma^2 \sim 7 \times 10^{-4} \text{ \AA}^2$  instead of  $\sim 2 \times 10^{-7} \text{ \AA}^2$  for PCMO). The CO-OO remains long-ranged in all the RCMO crystals, even when a small amount of Ca is substituted with Sr. For example, in the insets of Fig. 1, we show the [001] zone-axis electron diffraction (ED) patterns of  $\text{Eu}_{0.5}(\text{Ca}_{1-y}\text{Sr}_y)_{1.5}\text{MnO}_4$  (ECSMO) obtained at 80 K. In addition to the fundamental spots (associated with the  $\text{K}_2\text{NiF}_4$  structure), the EDPs include superlattice (SL) spots, associated with the CO-OO. The sharpness and the modulation wave vector however are dependent on the Sr concentration (see below). The different panels of Fig. 1 illustrate the changes in the microstructure related to the CO-OO with increasing Sr content. These dark-field (DF) images were recorded at 80K, using the SL reflection marked by the

arrow in the electron diffraction patterns (EDPs). The bright regions in Fig. 1 correspond to regions where the CO-OO occurs. For  $y=0.1$  large CO-OO domains are observed. On increasing Sr content, the size of the CO-OO domains decreases ( $y=0.25$ ), until the CO-OO becomes short-ranged ( $y=0.4$ ).

The order-disorder in the charge-orbital sector also affects macroscopic properties such as the magnetization or ac-susceptibility, as well as the electrical resistivity. For example, the disappearance of the long-range CO-OO state is observed in the  $T$ -dependence of the electrical resistivity, as shown in the upper panel of Fig. 2 for  $\text{Pr}_{0.5}(\text{Ca}_{1-y}\text{Sr}_y)_{1.5}\text{MnO}_4$  (PCSMO). The  $\rho(T)$  curves show a clear (and hysteretic in temperature) inflection near the CO-OO transition temperature  $T_{\text{CO-OO}}$  up to  $y=0.5$ , for which no CO-OO phase transition occurs, as confirmed by the ED data.  $T_{\text{CO-OO}}$  is also clearly observed in the  $\chi(T)$  curves as the sharp peak arising from the quenching of the FM spin fluctuation. Figure 2 shows the temperature dependence of the in-phase component of the ac-susceptibility  $\chi'$  for some of the single crystals.  $T_N$  is however difficult to identify, as seen for example in the  $\chi(T)$  curves of the well known LSMO[12]. As seen in the left lower panel of Fig. 2, in the RCMO crystals with small disorder ( $\sigma^2 < 1 \times 10^3 \text{ \AA}^2$ ) and relatively small average ionic radius ( $r_A \sim 1.16\text{-}1.18 \text{ \AA}$ ), a sharp peak marking  $T_{\text{CO-OO}}$  is observed above 320K. At lower temperatures, near 200K, a broader peak is observed. This broader peak does not correspond to  $T_N$  for long-range spin order, which is  $\sim 120\text{-}130\text{K}$  in these crystals[13]. An inflection (more clearly seen in the  $T$ -derivative of  $\chi'(T)$ ) can be seen in the vicinity of these temperatures, which was found to coincide with the  $T_N$  determined by diffraction techniques[13]. The broad maximum near 200K may thus indicate the development of in-plane AFM correlation, rather than the long-ranged phase AFM transition. We refer in the following to this broad peak as  $T_S^*(ab)$ . In the RSMO crystals, with larger  $r_A$  ( $\sim 1.28 \text{ \AA}$ ) and bandwidth, only the susceptibility of LSMO (the right lower panel of Fig. 2) shows the  $T_{\text{CO-OO}}$  peak, as well as a bump near 150K which may reflect the above mentioned in-plane spin correlation. As the variance (quenched disorder) increases with substitution of the La ions with Pr, only a broad peak is observed at high temperatures, together with a broad frequency-dependent cusp at low temperatures[16]. We now compare these observations with the electron diffraction data. In the EDPs collected as a function of temperature, the superlattice spots associated with the CO-OO are observed for all the RSMO crystals (one such spot is marked with an arrow in the EDP of ECMO shown in the corner of the top-left panel of Fig. 1). However, these SL spots are sharp only for LSMO, and diffusive, more or less, for the crystals with larger  $R$ , confirming the short-ranged nature of the CO-OO correlation[15] as suggested by the absence of a sharp peak in  $\chi(T)$ . Thus in the half-doped case, the orbital

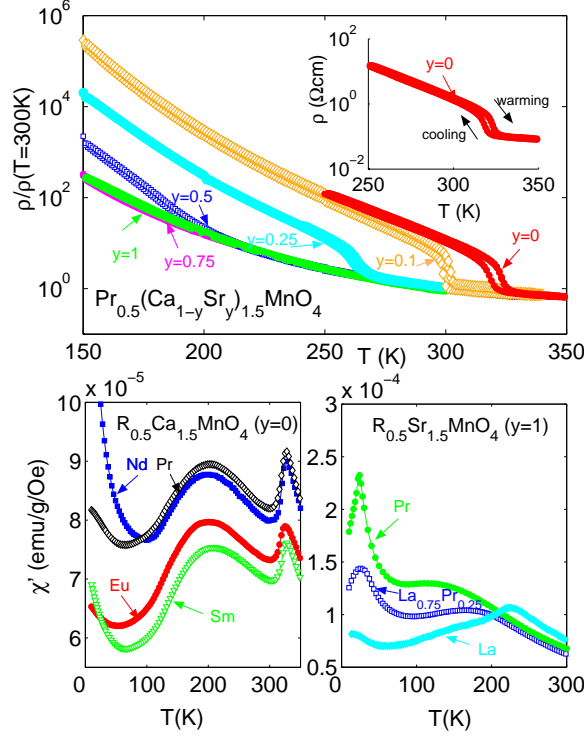


FIG. 2: (color online) Top panel: Temperature  $T$  dependence of the normalized in-plane resistivity  $\rho/\rho(T=300K)$  for  $\text{Pr}_{0.5}(\text{Ca}_{1-y}\text{Sr}_y)_{1.5}\text{MnO}_4$ . The inset shows the resistivity  $\rho$  of the crystal with  $y=0$  (PCMO) in absolute units. Lower panel: Temperature dependence of the in-plane component of the ac-susceptibility  $\chi'$  for some of the (left)  $\text{R}_{0.5}\text{Ca}_{1.5}\text{MnO}_4$  and (right)  $\text{R}_{0.5}\text{Sr}_{1.5}\text{MnO}_4$  crystals. The low-temperature upturn of  $\chi'(T)$  in the RCMO crystals is attributed to the  $4f$  moments of the  $R$  cations.

sector, as the master, controls the spin sector, as the slave, determining the spatial extent of its correlation as well.

The distinction between long-range and short range CO-OO is investigated in more detail, as a function of the bandwidth ( $r_A$ , or the Sr concentration  $y$ ) in Fig. 3. The top panel of Fig. 3 shows the variation of the lattice parameters of ECSMO, estimated at high temperatures ( $> T_{\text{CO-OO}}$ ) from the single-crystal x-ray diffraction. The  $a$ - and  $c$ -axis parameters decrease significantly with decreasing  $y$ , down to  $y=0.25$ . These crystals have a tetragonal  $I4/mmm$  structure similar to those of the RSMO crystals. For  $y < 0.25$ , the structure is orthorhombically distorted[16]. However, this structural transition does not coincide with the appearance of the long-range CO-OO order. The  $\chi(T)$  and  $\rho(T)$  curves suggest that the CO-OO order becomes short-ranged near  $y=0.4$ . This is confirmed by the ED data, as illustrated in the middle panel of Fig. 3. The half-width at half-maximum (HWHM) of the CO-OO superlattice spots in the EDPs is proportional to the inverse of the CO-OO

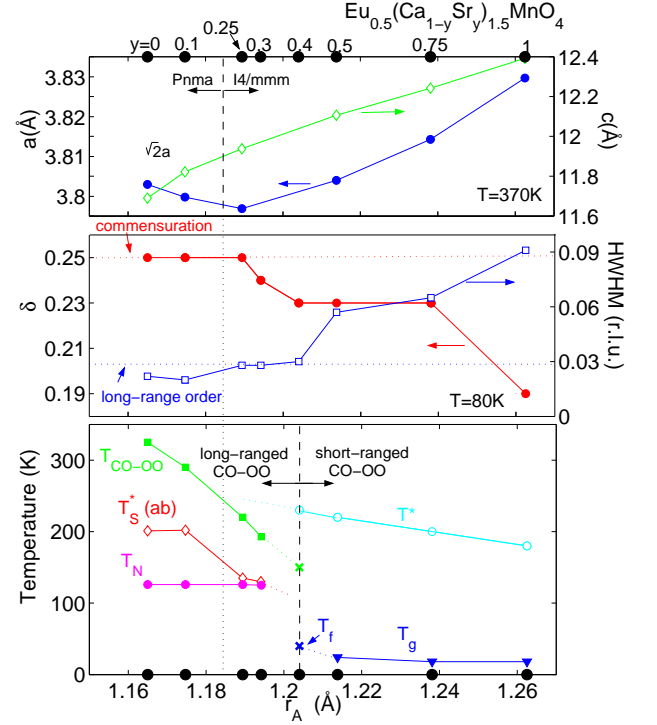


FIG. 3: (color online) Average ionic radius  $r_A$  dependence of selected physical properties of  $\text{Eu}_{0.5}(\text{Ca}_{1-y}\text{Sr}_y)_{1.5}\text{MnO}_4$ . Top:  $a$ - and  $c$ -axis lattice parameters;  $a \sim b$  for the crystals with  $Pnma$  structure. Middle: Modulation wave vector  $\delta$  and half-width at half-maximum HWHM of the superlattice reflection intensity profile obtained from electron diffraction (ED) at  $T = 80K$ . Bottom: the electronic phase diagram of  $\text{Eu}_{0.5}(\text{Ca}_{1-y}\text{Sr}_y)_{1.5}\text{MnO}_4$  (see main text for the definitions of the different labels). The crosses mark features in  $\rho(T)$  or  $\chi(T)$  curves, which do not necessarily correspond to phase transitions.

correlation length  $\xi_{\text{CO-OO}}$ . In the case of  $y=0.4$ , the HWHM is relatively small, however dark-field imaging reveal the short-ranged nature of the CO-OO order (c.f. Fig. 1). As  $y$  increases above 0.4, the HWHM gradually increases, i.e.  $\xi_{\text{CO-OO}}$  gradually decreases, down to the nanometer-scale[10]. The modulation wave vector of the SL spots also varies with  $r_A$  (or  $y$ ): it is commensurate ( $\delta=1/4$ ) up to  $y=0.25$ , and becomes incommensurate for  $y=0.3$ , although the CO-OO order is still long-ranged. It remains incommensurate for  $y \geq 0.4$  (short-range CO-OO order). The variation of the magnetic, and electrical properties of ECSMO are summarized in the bottom panel of Fig. 3.  $T^*$  marks the appearance of diffuse superlattice spots in the EDPs (i.e. CO-OO correlation)[15], while  $T_{\text{g}}$  is the SG phase transition temperature, obtained from the dynamical scaling of the  $T_{\text{f}}(f)$  freezing data of  $\chi(T, f)$ [6, 10]. In the case of the crystal with  $y=0.4$ , no true SG phase transition is found, albeit glassiness below  $T_{\text{f}} \sim 40K$ . While  $T_{\text{CO-OO}}$  largely varies with  $r_A$ ,  $T_{\text{N}}$  is relatively unchanged for all

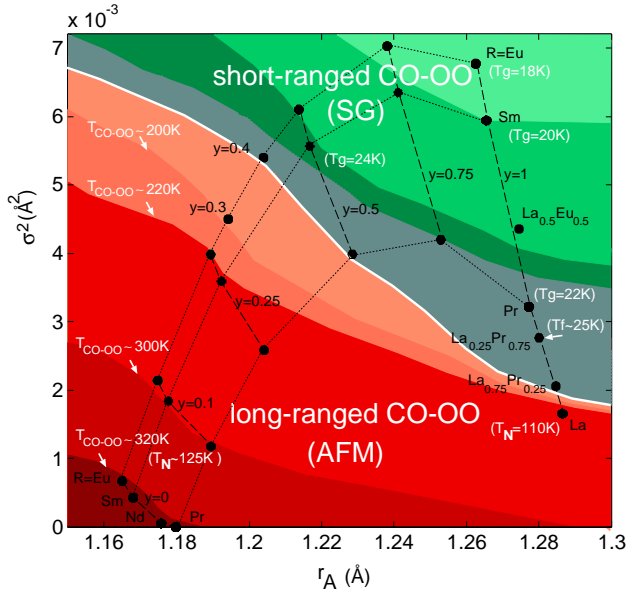


FIG. 4: (color online) Electronic phase diagram of  $R_{0.5}(\text{Ca}_{1-y}\text{Sr}_y)_{1.5}\text{MnO}_4$  in the plane of the average ionic radius  $r_A$  and the variance  $\sigma^2$ . Dashed lines connect the crystals with the same Sr content  $y$ , while dotted line connect crystals with the same  $R$  cation. Data of the CO-OO (the CO-OO transition temperature  $T_{\text{CO-OO}}$ ) and magnetic (the spin-glass (SG) phase transition temperature  $T_g$ , the freezing temperature  $T_f$ , and the antiferromagnetic (AFM) transition temperature  $T_N$ , in parenthesis) are included.

the crystals with long-range CO-OO order.

The schematic phase diagram presented in Fig. 3 can be also plotted as a function of  $\sigma^2$ . The resulting diagram is very similar, as both  $r_A$  and  $\sigma^2$  vary significantly with  $y$ . It hence makes sense to draw a global phase diagram in the planes of  $r_A$  and  $\sigma^2$  to take into account the effects of the variation of both bandwidth and quenched disorder. Such a “bandwidth-disorder” phase diagram is drawn in Fig. 4, using the ac-susceptibility, resistivity, and electron diffraction data, which was found to complement each other in the above. This phase diagram is reminiscent of the diagram obtained for the 3D perovskite case[2] in the small bandwidth area (for larger  $W$ , FM is observed in the perovskite case). In both cases, the long-range CO-OO order is replaced by a short-range “CE-glass” state (SG state) in the presence of large quenched disorder [6, 10]. However, the first-order like transition between the CO-OO and CE-glass phases observed in the perovskite case[4] does not occur in the layered systems. As indicated by the ED results, the CO-OO correlation length continuously decreases as the quenched disorder increases. Since there is a clear co-variation between the CO-OO correlation length and size of the “superspins” involved in the SG state, the latter of which was determined by the dynamical scaling of the  $\chi(T, f)$  data[10, 15], these groups of coherent spins may

be viewed as broken pieces of the CO-OO FM zig-zag chains of the CE-type structure.

To summarize, we have established for the first time the intrinsic bandwidth-disorder phase diagram of the half-doped layered manganites using high-quality single-crystals. As in the perovskite case, the CE-glass state occupies a large area of the diagram. Many specimens were found to exhibit a long-range CO-OO, with a  $T_{\text{CO-OO}}$  tunable around room-temperature and above by the bandwidth and/or disorder. The macroscopic phase separation, or ferromagnetic phases, sometimes reported in studies on polycrystals is not observed. Remarkably, the present diagram is very similar to that of the narrow-bandwidth perovskites, in spite of the dimensionality difference. However, in the present 2D layered case, the gradual decrease of the CO-OO correlation length as a function of bandwidth or disorder occurs, instead of the first-order-like collapse observed in the 3D case.

- 
- [†] Now at: Department of Microelectronics and Applied Physics, Condensed Matter Physics group (KMF), Royal Institute of Technology (KTH), Electrum 229, SE-164 40 Kista, Sweden. Electronic address: rmathieu@kth.se
- [1] Y. Tokura and N. Nagaosa, *Science* **288**, 462 (2000).
- [2] Y. Tomioka and Y. Tokura, *Phys. Rev. B* **70**, 014432 (2004).
- [3] Z. Jirák, S. Krupicka, Z. Simsa, M. Dlouhá, and Z. Vratislav, *J. Magn. Magn. Mater.* **53**, 153 (1985).
- [4] D. Akahoshi, M. Uchida, Y. Tomioka, T. Arima, Y. Matsui, and Y. Tokura, *Phys. Rev. Lett.* **90**, 177203 (2003).
- [5] H. Aliaga, D. Magnoux, A. Moreo, D. Poilblanc, S. Yunoki, and E. Dagotto, *Phys. Rev. B* **68**, 104405 (2003).
- [6] R. Mathieu, D. Akahoshi, A. Asamitsu, Y. Tomioka, and Y. Tokura, *Phys. Rev. Lett.* **93**, 227202 (2004).
- [7] N. Takeshita, C. Terakura, D. Akahoshi, Y. Tokura, and H. Takagi, *Phys. Rev. B* **69**, 180405(R) (2004).
- [8] B. J. Sternlieb, J.P. Hill, U.C. Wildgruber, G.M. Luke, B. Nachumi, Y. Moritomo, and Y. Tokura, *Phys. Rev. Lett.* **76**, 2169 (1996).
- [9] M. Ibarra, R. Retoux, M. Hervieu, C. Autret, A. Maignan, C. Martin, and B. Raveau, *J. Solid State Chem.* **170**, 361 (2003).
- [10] R. Mathieu, A. Asamitsu, Y. Kaneko, J. P. He, and Y. Tokura, *Phys. Rev. B* **72**, 014436 (2005).
- [11] J. P. Attfield, *Chem. Mater.* **10** 3239 (1998).
- [12] Y. Moritomo, Y. Tomioka, A. Asamitsu, Y. Tokura, and Y. Matsui, *Phys. Rev. B* **51**, R3297 (1995).
- [13] D. J. Huang et al., unpublished.
- [14] The broad peak at high- $T$  vanishes near  $R=\text{Eu}$ , which shows a sharp cusp at low  $T$ . The crystals with long-range CO-OO have no  $f$ -dependent  $\chi'(T)$ , and  $\chi''(T)$  is negligible. On the other hand, the crystals with short-range CO-OO show some glassiness or well-defined SG phase transitions related to the sharp cusps in  $\chi'(T)$ .
- [15] M. Uchida, R. Mathieu, J. P. He, Y. Kaneko, A. Asamitsu, Y. Tomioka, Y. Matsui, and Y. Tokura, unpublished.
- [16] These crystals adopt the  $Pnma$  structure, with nearly

identical  $a$  and  $b$  lattice parameters; the tilting of the  $\text{MnO}_6$  octahedra yields smaller Mn-O-Mn bond angles.